Supporting Information for

Towards a Comprehensive Understanding of Visible-Light Photogeneration of Hydrogen from Water Using Cobalt(II) Polypyridyl Catalysts

Rony S. Khnayzer,[a,g,†] V. Sara Thoi,[b,d†] Michael Nippe,[b,d,] Amanda E. King,[b,d] Jonah W. Jurss,[b,d] Karim A. El Roz,[a] Jeffrey R. Long,[b,e,*] Christopher J. Chang,[b,c,d,f,*] and Felix N. Castellano[a,*]

[a]Department of Chemistry, North Carolina State University, Raleigh, NC 27695-8204, USA. [b]Department of Chemistry and [c]Molecular and Cell Biology, University of California, Berkeley, California 94720, USA; [d]Chemical Sciences Division and [e]Materials Sciences Division, Lawrence Berkeley National Laboratory, Berkeley, California 94720, USA; [f]Howard Hughes Medical Institute, University of California, Berkeley, California 94720, USA; [g]Department of Natural Sciences, Lebanese American University, Chouran, Beirut 1102-2801, Lebanon.

Corresponding Authors

*e-mail: fncastel@ncsu.edu, chrischang@berkeley.edu, jrlong@berkeley.edu.

Author Contributions

† R.S.K. and V.S.T. contributed equally to this work.

Experimental Section

General. All reagents were purchased from Sigma-Aldrich or Alfa Aesar and used without further purification. D_2O (99 %) was purchased from Cambridge Isotope Laboratories. Water used in photocatalytic experiments was deionized using a Barnstead Nanopure system. The compounds bpyPY2OMe,[1] complex **3**,[1] complex **5**,[2] bpyPY2OH,[3] ethyl-CF3-pyridine,[4] 1-(2-(4-trifluoromethyl)-pyridyl)-1-(6-2,2'-bipyridyl)ethane[4], pr-bpy2[5] were prepared according to published procedures. Literature methods were also used to synthesize 1,1-bis(2-pyridyl)ethane,[6] 2,2'-(1-(6-fluoropyridin-2-yl)ethane-1,1-diyl)dipyridine (F-PY3),[7] and $[Co(PY5Me_2)(H2O)]^{2+}$.[8] Solvents were dried using a commercial SPS from jcmeyer-solventsystems. Infrared spectra were obtained on a Nicolet Avatar 360 FTIR spectrometer equipped with an attenuated total reflectance (ATR) accessory. Carbon, hydrogen, and nitrogen analyses were obtained from the Microanalytical Laboratory at the University of California, Berkeley. ^{1}H, and ^{13}C-NMR spectra were obtained using either a Bruker AVQ-400, AVB-300, or AVANCEIII 500 instrument and peaks were referenced to residual solvent peaks. Positive mode electrospray ionization mass spectrometry (ESI-MS) measurements were performed using a quadrupole time-of-flight mass spectrometer (Q-tof Premier, Waters, Milford, MA).

Syntheses.

bpyPY2Me. A procedure analogous to the synthesis of 2,6-bis[(2-pyridyl)ethyl]pyridine ($PY5Me_2$) was employed. Under a nitrogen atmosphere, 1,1-bis(2-pyridyl)ethane (2.35 g, 12.8 mmol) was dissolved in dry THF (50 mL) and cooled to -78 °C. A solution of n-butyllithium (5.10 mL, 12.8 mmol) was added slowly via syringe, and the resulting red solution was allowed to stir at -78 °C for 45 min. Under a positive flow of nitrogen, 6-bromo-2,2'-bipyridine (2.00 g, 8.50 mmol) was added in one portion. The reaction mixture was slowly warmed to room temperature, and then refluxed for 48 hours after which the reaction mixture was cooled to room temperature and quenched by the addition of H_2O (50 mL). The solvent was removed by rotary evaporation, and the resulting residue suspended in CH_2Cl_2. The organic phase was washed with water (3 · 150 mL) and brine (100 mL). The CH_2Cl_2 was removed under reduced pressure and the resulting yellow-brown oil was suspended in CH_2Cl_2 (5 mL) and pentane (20 mL), and cooled overnight at -35 °C. 2.5 g of a light brown solid was obtained (86.9% yield). ^{1}H-NMR (CD_3Cl, 300 MHz): δ 8.62 (m, 3H), 8.24 (d, J = 7.8 Hz, 1H), 8.17 (d, J = 8.1 Hz, 1H), 7.72 (d, J = 7.8 Hz, 1H), 7.65 (d, J = 8.1 Hz, 1H), 7.56 (m, 2H), 7.25-7.08 (m, 6H), 2.42 (s, 3H). ^{13}C-NMR (CD_3Cl, 100 MHz): δ 166.21, 164.75, 156.53, 156.63, 148.91, 148.81, 136.96, 136.71, 135.86, 123.68, 121.28, 121.20, 118.33, 60.36, 27.24. Anal. Calcd. for $C_{22}H_{18}N_4$: C, 78.08%; H, 5.36%; N, 16.56%. Found: C, 77.70%; H, 5.24%; N, 16.41%. ESI-TOF MS (m/z, amu): 339.16 $[M+H]^+$. IR (neat, cm^{-1}): 1578 (m), 1560 (s), 1467 (s), 1453 (m), 1427 (s), 1404 (w), 1364 (w), 1294 (w), 1265 (w), 1250 (w), 1160 (m), 1148 (w), 1120 (w), 1108 (m), 1091 (m), 1074 (w), 1067 (m), 1046 (m), 991 (m), 968 (w), 926 (w), 892 (w), 881 (w), 864 (w), 800 (w), 786 (m), 777 (s), 762 (m), 752 (s), 744 (s), 709 (w), 674 (s), 654 (s), 628 (m), 622 (m), 599 (w), 579 (m), 522 (w), 478 (w).

bpy(PY-CF_3)2Me. A solution of freshly prepared LDA (from diisopropylamine (560 μL, 3.95 mmol) and butyllithium (2.5 M in hexanes, 1.58 mL, 3.95 mmol)) in THF (25 mL) was added to a solution of 1-(2-(4-trifluoromethyl)-pyridyl)-1-(6-2,2'-bipyridyl)ethane (1.30 g, 3.95 mmol) in THF (30 mL) at -78 °C, and the resulting dark red mixture was stirred at -78 °C for 1 h. After addition of a solution of 2-bromo-4-trifluoromethyl-pyridine (0.89 g, 3.95 mmol) in THF (10 mL), the mixture was allowed to warm to room temperature and subsequently stirred at reflux for

18 h. After cooling to room temperature, quenching with saturated $NaHCO_3$ (aq) solution (50 mL), extraction into CH_2Cl_2 (3 × 80 mL), and drying of the combined organic phases over $MgSO_4$, the solvents were removed under reduced pressure. Recrystallization from hexanes yielded 1.43 g (80%) of product. ^{1}H NMR ($CDCl_3$, 500 MHz): δ 8.76 (d, 2H, J = 5 Hz), 8.65 (d, 1H, J = 4.5 Hz), 8.34 (d, 1H, J = 8 Hz), 8.07 (d, 1H, J = 8 Hz), 7.82 (t, 1H, J = 8Hz), 7.70 (t, 1H, J = 8 Hz), 7.50 (s, 2H), 7.40 (d, 2H, J = 4.5 Hz), 7.28 (m, 2H), 2.42 (s, 3H). ^{13}C NMR (CD_3Cl, 125 MHz) δ 167.11, 162.94, 155.91, 154.97, 149.52, 148.99, 138.09 (q, J = 34 Hz), 137.58, 136.75, 124.00, 123.74, 122.92 (q, J = 272 Hz), 121.03, 119.56 (q, J = 3.6 Hz), 118.93, 117.10 (q, J = 3.3 Hz), 60.54, 27.08. ESI-TOF MS (m/z, amu): 475.13 $[M+H]^+$. IR (neat, cm^{-1}): 1611 (w), 1579 (m), 1561 (m), 1470 (w), 1454 (m), 1431 (m), 1401 (m), 1392 (m), 1370 (w), 1327 (s), 1291 (w), 1294 (w), 1222 (w), 1200 (w), 1173 (s), 1164 (2), 1132)s), 1087 (s), 1066 (m), 1042 (w), 990 (m), 982 (w), 969 (w), 904 (m), 892 (m), 863 (m), 843 (m), 829 (w), 818 (w), 793 (m), 775 (m), 765 (s), 752 (m), 728 (w), 718 (w), 690 (m), 666 (s), 643 (m), 626 (m), 607 (w), 585 (w), 558 (w), 510 (w), 469 (w), 455 (w).

2-(1,1-Bis(2-pyridyl)ethyl)-6-(1-(2-pyridyl)methyl)pyridine ($PY4MeH_2$). To a solution of 250 μL of 2-picoline (0.236 g, 2.53 mmol) in 100 mL of THF at -78°C was slowly added 1.2 mL of 2.5 M *n*-butyllithium (3 mmol) in hexanes.The resulting red solution was stirred for 30 min before 2,2'-(1-(6-fluoropyridin-2-yl)ethane-1,1-diyl)dipyridine (F-PY3) (0.593 g, 2.13 mmol) was added. After the solution was allowed to stir for 12 h, the reaction was quenched with 50 mL of water and the organic components were extracted with DCM (100 mL x 3). The organics were combined, washed with water, and dried with Na_2SO_4. The solution was evaporated to dryness and the tan oil was purified by alumina chromatography using 2% MeOH/DCM as the eluent. The final product was a tan oil (0.337 g, 0.96 mmol, 45%). ^{1}H NMR (500 MHz, $CDCl_3$): δ 8.54 (d, *J* = 3.7 Hz, 2H), 8.45 (d, *J* = 4.2 Hz, 1H), 7.56 – 7.37 (m, 4H), 7.12 – 7.02 (m, 6H), 6.99 (d, *J* = 8.0 Hz, 2H), 6.91 (d, *J* = 8.0 Hz, 2H), 4.22 (s, 2H), 2.30 (s, 3H). ^{13}C NMR (125 MHz, $CDCl_3$): δ 166.15, 165.09, 159.76, 158.12, 148.90, 148.62, 136.60, 136.17, 135.74, 123.88, 123.77, 121.24, 121.07, 120.83, 120.78, 60.12, 53.46, 47.24, 27.15. Anal. Calcd for $C_{23}H_{20}N_4$: C, 78.38; H, 5.72; N, 15.90. Found: C, 78.06; H, 5.73; N, 15.64. EI-HRMS ($[MH]^+$) *m/z* calcd for $C_{23}H_{20}N_4$ 352.1688, found 352.1678.

2-(1,1-Bis(2-pyridyl)ethyl)-6-(1-(2-pyridyl)ethyl)pyridine ($PY4Me_2H$). The synthesis of **3** followed the procedure of **2**, starting with 231 μL (0.937 mmol) of 2- ethylpyridine, 745 μL of *n*-butyllithium (1.9 mmol), and 0.514 g of **F-PY3** (1.84 mmol) to yield a tan oil product (0.18 g, 0.50 mmol, 27%). ^{1}H NMR (400 MHz, $CDCl_3$) δ 8.56 (d, *J* = 5.0 Hz, 2H), 8.46 (d, *J* = 4.1 Hz, 1H), 7.58 – 7.41 (m, 4H), 7.13 – 7.06 (m, 5H), 7.13 – 7.06 (m, 5H), 4.36 (q, *J* = 7.2 Hz, 1H), 2.32 (s, 3H), 1.60 (d, *J* = 7.2 Hz, 3H). ^{13}C NMR (126 MHz, $CDCl_3$) δ 166.31, 166.23, 164.76, 164.39, 162.09, 148.57, 148.51, 136.61, 136.18, 135.61, 123.90, 122.53, 121.23, 121.05, 121.02, 120.46, 119.96, 60.19, 49.84, 27.03, 19.98. Anal. Calcd for $C_{24}H_{22}N_4 \cdot 0.25(H_2O)$: C, 77.71; H, 6.11; N, 15.10. Found: C, 77.54; H, 6.30; N, 14.88. EI-HRMS ($[MH]^+$) *m/z* calcd for $C_{24}H_{22}N_4$ 366.1844, found 366.1844.

2-(1,1-Bis(2-pyridyl)ethyl)-6-(2-(2-pyridyl)isopropyl)pyridine ($PY4Me_3$). To a solution of diisopropylamine (1.2 mL, 0.860 g, 8.51 mmol) and KO^tBu (0.983 g, 8.78 mmol) in 100 mL of THF at -78°C was slowly added 5.5 mL of 1.6 M *n*-butyllithium (8.8 mmol) in hexanes and the red solution was stirred for 30 min before 2-isopropylpyridine (0.874 g, 7.22 mmol) was added. The solution was again allowed to stir for 30 min before F-PY3 (2.00 g, 7.20 mmol) was added. After the solution was allowed to stir for 12 h, the reaction was quenched with 50 mL of water

and the organic components were extracted with EtOAc (100 mL x 3). The organics were combined, washed with water, and dried with Na_2SO_4. The solution was evaporated to dryness and the tan oil was purified by alumina chromatography using 30% EtOAc/hexanes as the eluent. The final product was a tan oil (0.800 g, 2.10 mmol, 29%). ^{1}H NMR (500 MHz, $CDCl_3$) δ 8.54 (d, *J* = 4.0 Hz, 2H), 8.49 (d, *J* = 4.0 Hz, 1H), 7.51 – 7.43 (m, 4H), 7.08 – 7.00 (m, *5*H), 6.96 (d, *J* = 7.6 Hz, 1H), 6.92 (d, *J* = 8.0 Hz, 2H), 2.31 (s, *3*H), 1.65 (s, 6H). ^{13}C NMR (125 MHz, $CDCl_3$): δ 167.77, 166.37, 166.15, 163.88, 148.46, 148.22, 136.51, 135.80, 135.53, 123.98, 121.75, 120.97, 120.66, 119.71, 118.01, 60.15, 48.15, 28.09, 26.87. Anal. Calcd for $C_{25}H_{24}N_4$: C, 78.92; H, 6.36; N, 14.73. Found: C, 78.57; H, 6.46; N, 14.63. EI-HRMS ($[MH]^+$) *m/z* calcd for $C_{25}H_{24}N_4$ 380.2001, found 380.2000.

1,3-di([2,2'-bipyridin]-6-yl)propane (pr-bpy$_2$). This ligand was prepared according to a published procedure.[5] Yield = 550 mg (27%). ^{1}H NMR (400 MHz, $CDCl_3$): δ 8.76-8.62 (m, 2H), 8.47 (d, *J* = 8.0 Hz, 2H), 8.20 (d, *J* = 7.8 Hz, 2H), 7.79 (td, *J* = 7.7, 1.9 Hz, 2H), 7.72 (t, *J* = 7.8 Hz, 2H), 7.29 (dd, *J* = 7.3, 4.5 Hz, 2H), 7.20 (d, *J* = 7.7 Hz, 2H), 2.99 (t, *J* = 7.6 Hz, 4H), 2.38 (p, *J* = 7.7 Hz, 2H). ^{13}C NMR (101 MHz, $CDCl_3$): δ 161.23 (s), 156.49 (s), 155.42 (s), 149.00 (s), 136.99 (s), 136.71 (s), 123.42 (s), 122.83 (s), 121.13 (s), 118.21 (s), 37.76 (s), 29.29 (s). ESI-HRMS ($[M]^+$) m/z calc. for [**1**+H^+], 353.1761, Found, 353.1758.

[Co(bpyPY2Me)(CH_3CN)(CF_3SO_3)](CF_3SO_3) (1). Complexation of bpyPY2Me (100 mg, 296 μmol) with $Co(CH_3CN)_2(CF_3SO_3)_2$ (105.5 mg, 296 μmol) was carried out in 3 mL of acetonitrile. After 2 hours of stirring, 15 mL of ether was added to the red-orange solution and recrystallization resulted in the formation of 150 mg of red-orange blocks (68.8 % yield). X-ray quality crystals were obtained via vapor diffusion of diethyl ether into an acetonitrile solution of [Co(bpyPY2Me)(CH_3CN)(CF_3SO_3)](CF_3SO_3) Anal. Calcd. for $C_{26}H_{21}CoF_6N_5O_6S_2$: C, 42.40%; H, 2.87%; N, 9.51%. Found: C, 42.14%; H, 2.61%; N, 9.21%. ESI-TOF MS (m/z, amu): 442.08 [Co(bpyPY2Me)(CHO_2)]$^+$, 546.04 [Co(bpyPY2Me)(CF_3SO_3)]$^+$. IR (neat, cm^{-1}): 1596 (m), 1579 (w), 1565 (w), 1478 (w), 1465 (m), 1450 (m), 1441 (m), 1397 (w), 1372 (w), 1306 (m), 1294 (s), 1266 (s), 1235 (s), 1226 (s), 1179 (m), 1159 (m), 1141 (s), 1119 (m), 1073 (w), 1055 (w), 1028 (s), 976 (w), 914 (w), 871 (w), 857 (w), 805 (m), 779 (s), 763 (m), 740 (w), 708 (w), 665 (m), 634 (s), 599 (w), 572 (m), 516 (s).

[Co(bpy(PY-CF_3)2Me)(CH_3CN)$_2$)](CF_3SO_3)$_2$ (2). Utilizing analogous reactions conditions as for the synthesis of **1**, complex **2** is obtained in 78 % yield. Anal. Calcd. for $C_{30}H_{22}CoF_{12}N_6O_6S_2$: C, 39.44%; H, 2.43%; N, 9.20%. Found: C, 38.99%; H, 2.27%; N, 8.75%. ESI-TOF MS (m/z, amu): 578.06 [Co(bpy(PY-CF_3)2)(CHO_2)]$^+$, 682.01 [Co((bpy(PY-CF_3)2)(CF_3SO_3)]$^+$. IR (neat, cm^{-1}): 1624 (w), 1600 (w), 1568 (w), 1488 (w), 1454 (m), 1406 (m), 1374 (w), 1332 (s), 1293 (m), 1266 (s), 1236 (s), 1226 (s), 1178 (s), 1139 (s), 1103 (s), 1083 (m), 1027 (s), 975 (w), 911 (m), 904 (w), 882 (w), 863 (w), 851 (m), 825 (w), 791 (w), 774 (m), 756 (m), 716 (w), 688 (m), 679 (m), 659 (w), 634 (s), 617 (m), 573 (m), 517 (s), 468 (m).

[Co(bpyPY2OH)(CH_3CN)(CF_3SO_3)](CF_3SO_3) (4). Utilizing analogous reactions conditions as for the synthesis of **1**, complex **4** is obtained in 56 % yield. Anal. Calcd. for $C_{25}H_{19}CoF_6N_5O_7S_2$: C, 40.66%; H, 2.59%; N, 9.48%. Found: C, 40.70%; H, 2.62%; N, 9.77%. ESI-TOF MS (m/z, amu): 444.06 [Co(bpyPY2OH)(CHO_2)]$^+$, 548.02 [Co(bpyPY2OH)(CF_3SO_3)]$^+$. IR (neat, cm^{-1}): 1599 (m), 1581 (w), 1565 (w), 1466 (w), 1449 (m), 1442 (w), 1365 (w), 1294 (s), 1238 (s), 1226 (s), 1185 (w), 1159 (s), 1148 (s), 1097 (w), 1085 (m), 1064 (w), 1029 (s), 972 (w), 942 (w), 934 (w), 899 (w), 823 (w), 810 (w), 784 (m), 772 (s), 759 (m), 715 (w), 675 (m), 666 (m), 634 (s), 574 (m), 516 (s), 498 (w).

[Co(pr-bpy$_2$)(SO$_3$CF$_3$)$_2$] (6). Acetonitrile (10 mL) was added to a solid mixture of pr-bpy2 (100 mg, 0.284 mmol) and $Co(CF_3SO_3)_2(CH_3CN)_2$ (125 mg, 0.284 mmol). The reaction was left to stir overnight at room temperature after which the mixture was concentrated. Diethyl ether diffusion into acetonitrile solutions yielded pink crystals suitable for x-ray crystallography. Yield = 141 mg (70%). Elem. Anal. Calc. for $C_{25}H_{20}CoF_6N_4O_6S_2$: C, 42.32; H, 2.84; N, 7.90. Found: C, 42.38; H, 2.64; N, 7.87. ESI-HRMS ([M]$^+$) *m/z* calc. for [Co(pr-bpy$_2$)(SO$_3$CF$_3$)$^+$], 560.0535, Found, 560.0525.

[Co(PY4MeH$_2$)(CH$_3$CN)(CF$_3$SO$_3$)](CF$_3$SO$_3$) (7). To a solution of **PY4MeH$_2$** (0.121 g, 0.34 mmol) in 5 mL of CH_3CN was added $Co(CF_3SO_3)_2(CH_3CN)_2$ (0.151 g, 0.34 mmol) and the pink solution was stirred for 8 h. The resulting solution was evaporated to obtain a pink precipitate and was quantitatively recrystallized by diffusing Et_2O into a concentrated solution of **7** in CH_3CN. Anal. Calcd for $C_{27}H_{23}N_5CoF_6O_6S_2 \cdot H_2O$: C, 42.19; H, 3.28; N, 9.11. Found: C, 41.97; H, 3.00; N, 8.71. ESI-HRMS ([M]$^+$) *m/z* calcd for $C_{26}H_{23}N_5CoF_3O_3S$ 560.0540, found 560.0548.

[Co(PY4Me$_2$H)(CH$_3$CN)(CF$_3$SO$_3$)](CF$_3$SO$_3$) (8). The synthesis of **8** followed the procedure of **7**, starting with 0.058 g (0.16 mmol) of **PY4Me$_2$H** and 0.070 g (0.16 mmol) of $Co(CF_3SO_3)_2(CH_3CN)_2$ to yield a pink product (0.111 g, 0.14 mmol, 90%). Anal. Calcd for $C_{26}H_{22}N_4CoF_6O_6S_2 \cdot H_2O$: C, 42.11; H, 3.26; N, 7.56. Found: C, 41.93; H, 3.39; N, 7.46. ESI-HRMS ([M]$^+$) *m/z* calcd for $C_{25}H_{22}N_4CoF_3O_3S$ 574.0705, found 588.0705.

[Co(PY4Me$_3$)(CH$_3$CN)](CF$_3$SO$_3$)$_2$ (9). The synthesis of **9** followed the procedure of **7**, starting with 0.030 g (0.079 mmol) of **PY4Me$_3$** and 0.035 g (0.079 mmol) of $Co(CF_3SO_3)_2(CH_3CN)_2$ to yield a pink product quantitatively. Anal. Calcd for $C_{27}H_{24}N_4CoF_6O_6S_2 \cdot H_2O$: C, 42.92; H, 3.47; N, 7.41. Found: C, 43.20; H, 3.47; N, 7.27.ESI-HRMS ([M]$^+$) *m/z* calcd for $C_{26}H_{24}N_4CoF_3O_3S$ 588.0853, found 588.0855.

Crystal Structure Determinations

Data collection was performed on single crystals coated with Paratone-N oil and mounted on Kaptan loops. The crystals were frozen under a stream of N_2 (100 K; Oxford Cryostream 700) during measurements. Data were collected using a Bruker APEX II QUAZAR diffractometer equipped with a Microfocus Sealed Source (Incoatec IμS; Mo-Kα λ = 0.71073 Å) and APEX-II detector. Raw data were integrated and corrected for Lorentz and polarization effects using Bruker APEX2 v. 2009.1.[9] Absorption corrections were applied using SADABS.[10] Space group assignments were determined by examination of systematic absences, E-statistics, and successive refinement of the structures. Structures were solved using direct methods and refined by least-squares refinement on F^2 followed by difference Fourier synthesis.[11] All hydrogen atoms were included in the final structure factor calculation at idealized positions and were allowed to ride on the neighboring atoms with relative isotropic displacement coefficients. Thermal parameters were refined anisotropically for all non-hydrogen atoms.

Photocatalytic Experiments. Hydrogen production measurements were performed in a home-built 16 well combinatorial apparatus.[12] Typically, 10 mL of total catalytic solution volume prepared in a 20 or 40 mL air-tight EPA vial (VWR Scientific) was irradiated from the bottom using a royal-blue LED (Philips, Luxeon Rebel series) mounted on a starboard (LXMS-PR01-0425-CT) whose output was passed through a Fraen narrow beam lens (12^o beam angle, FLP-N4-RE-HRF). The current passing through the LED was controlled by a home-built circuit board and could be adjusted between 450 and 800 mA. The optical power output at λ_{max} = 452 ± 10 nm was monitored using a power meter and this output (typically 540 mW @ 700 mA) was easily fine-tuned before each run. All experiments were performed at a constant rotation speed of 150

rpm controlled by an IKA orbital shaker. All reaction vials and LEDs were temperature controlled by aluminum blocks cooled using a circulating chiller. The temperature was set to ~ 20 °C in most reactions, unless otherwise stated. Solutions containing ascorbic acid/ascorbate (prepared by titration of ascorbic acid with NaOH) and the photosensitizer were thoroughly deaerated using a number of vacuum/argon pressurization cycles. The molecular cobalt catalysts were introduced under inert atmosphere and degassing was continued; finally terminated by equilibration to atmospheric pressure. Ar was also used in our system as an internal standard to get the percent of H_2 produced by MS. The vials are each connected to pressure transducers (SSI technologies, P51 pressure sensors) through a Teflon spacer by stainless steel fittings and to a universal gas analyzer (Stanford Research Systems, UGA-hydrogen) by capillary tubes. During the course of a given reaction, head space pressure is monitored in real-time using a multifunction data acquisition box (National Instruments, NI-USB-6210) and data were logged using LabVIEW SignalExpress software. After the end of each photocatalytic reaction, headspace sampling (100 μL) was performed using a Hamilton syringe followed by injection into a GC-8A (Shimadzu) equipped with a 5Å molecular sieves column and thermal conductivity detector (TCD) operated with Ar carrier gas. In addition, the headspace which was pressurized by H_2 buildup during the course of photocatalysis, was equilibrated to atmospheric pressure and the percent of H_2 relative to Ar was analyzed by MS. GC and MS data were calibrated against a certified Ar/H_2 standard (Praxair). Quantitative results of hydrogen were typically averaged and the processed pressure data were normalized to the final amounts of hydrogen measured. For the deuteration experiments, water was replaced by deuterium oxide, and the kinetics of hydrogen production was measured as well as gas mixture analysis was performed using MS. The calibration of the MS for D_2 and HD was done against standards produced following the reaction of Li metal with D_2O and H_2O:D_2O mixtures respectively and the calculations were based on the pressure buildup during the course of the reaction. Our method for D_2 and HD calibration was verified by obtaining identical sensitivity factors for H_2 when using the certified standards (Praxair) or following the reaction of Li with H_2O.

The measurements under 1 sun illumination were performed in a Pyrex 50 mL round-bottom. 25 mL of water containing the electron donor, sensitizer and catalyst was deaerated by freeze-pump-thaw technique and left under reduced argon pressure (~ 100 torr). The mixture was irradiated using a 300 W xenon arc lamp equipped with a water filter to decrease heat formation and an AM1.5G filter (Oriel) mounted in series with appropriate neutral density filters in order to obtain ~100 mW/cm^2 broadband optical output. The reaction was stirred at constant rate and the headspace was analyzed by injection into a GC at regular intervals.

Electrochemistry. Electrochemical measurements were performed in an inert atmosphere glovebox (MBraun) using 0.1 M $TBAPF_6$ as the supporting electrolyte in acetonitrile which was dried and degassed with an MBraun SPS solvent purification system. Cyclic voltammograms were measured using a standard three-electrode arrangement with a platinum disk working electrode, a Pt wire counter electrode, and an $Ag/AgNO_3$ reference electrode. The ferrocenium/ferrocene redox couple ($Fc^{+/0}$) was used as an internal reference. The spectra were recorded with a Bioanalytical Systems (BASi) Epsilon potentiostat. Aqueous electrochemistry was performed using glassy carbon disk, graphite rod, and Ag/AgCl/KCl as the working, auxiliary, and reference electrode, respectively.

Spectroelectrochemistry. Experiments were performed using the apparatus described above coupled to a 1 mm pathlength spectroelectrochemical cell (BASi). Pt mesh was used as the working electrode in conjunction with a $Ag/AgNO_3$ as reference, and a Pt wire as the counter

electrode. Solutions were prepared in acetonitrile containing 0.1 M $TBAPF_6$ supporting electrolyte. Controlled-potential electrolysis (CPE) was performed at potentials ~50-100 mV negative of the first reduction wave. Absorbance spectra were collected with a SI440 CCD spectrometer every 30-60 seconds during the CPE until current ceased to flow. Relevant extinction coefficients of the reduced species were calculated using the Beer-Lambert law and assumed complete 1 e^- reduction of the initial compound.

Static Spectroscopic Measurements. Absorption spectra were acquired using a Cary 50 or an Agilent 8453 diode array spectrophotometer. Static emission spectra were collected using a FL/FS920 spectrofluorimeter (Edinburgh Instruments) equipped with a 450 W Xe arc lamp and a Peltier cooled, red sensitive PMT (R2658P, Hamamatsu). All emission spectra were corrected for detector response. For each measurement, optically dilute (OD = 0.1-0.2) solutions were excited into the lowest energy absorption feature and solutions were degassed by purging with a stream of Ar gas for a minimum of 30 minutes and the head space of the solutions were maintained under positive Ar pressure during data acquisition.

Dynamic Spectroscopic Measurements. Time-resolved photoluminescence and transient absorption data were collected with an LP920 laser flash photolysis system from Edinburgh Instruments. The excitation pump source was the Vibrant LD 355 II Nd:YAG/OPO system (OPOTEK). Data acquisition was controlled by the LP920 software program (Edinburgh Instruments). Samples were prepared with an optical density of 0.1 - 0.2 at the excitation wavelength for emission measurements and 0.3-0.5 at the excitation wavelength for transient absorption measurements. These samples were degassed identically as stated above. Kinetic traces were collected with a PMT (R928 Hamamatsu) and transient absorption difference spectra were collected using an iStar ICCD camera (Andor Technology). The associated kinetic traces were modeled using Origin 8.1. Electron transfer cage escape efficiencies were calculated using relative actinometry as described previously.

Quantum Yield of Hydrogen Production. These measurements have been conducted over 12 samples. The first 9 samples were excited using the LED light sources (452 ± 10 nm), and 3 other samples were excited using the 442nm line isolated from a He/Cd laser. For each light source the power density was varied and measurements were taken at 3 different incident power densities. For the LED, both diluted (15 μM) and concentrated samples (%T = 0, $[Ru(bpy)_3]^{2+}$ = 3.3 x 10^{-4} M) gave similar results. The concentration of **1** was 40 μM in all QY experiments and $[H_2A/HA^-]$ = 0.5 M, pH 4 to ensure > 80 % quenching of $[Ru(bpy)_3]^{2+}$. For the laser measurement, the power density before and after the sample was measured to get the absorbed power by the system. Since two photons are needed to produce one H_2, these quantum yields are based on two photons absorbed.

$\Phi = 2 \times n_{H2} \times n\ (photons)^{-1}$

Where n_{H2} is the number of hydrogen produced as measured in the headspace of the reactors, and $n_{photons}$ is the number of photons absorbed by the samples as calculated from the following formula: $n_{photons} = P_{abs} \times t \times E_{photon}^{-1} \times N_A^{-1}$; where P_{abs} is the power absorbed (W), t is irradiation time in (s) and E_{photon} is the energy of a photon (J) assuming monochromatic light, and N_A is Avogadro's number.

Φ = 7.5 ± 0.8 % (LED) and Φ = 7.6 ± 0.6 % (laser).

Cage Escape Calculations. The cage escape yield (Φ_{CE}) was calculated from transient absorption kinetic decay analysis using $[Ru(bpy)_3]^{2+}$ in water as actinometer.[13,14]

$$\Phi_{CE} = \frac{\Delta A_{sample} / \Delta\epsilon_{sample} \times (1 - 10^{-A_{actinometer}})}{\Delta A_{actinometer} / \Delta\epsilon_{actinometer} \times (1 - 10^{-A_{sample}}) \times fraction\ quenched}$$

Where ΔA_{sample} is the maximum of the decay of the radical anion, $\Delta\varepsilon_{sample}$ was estimated from spectroelectrochemical measurement leading to the extinction coefficient at a particular wavelength, $\Delta A_{actinometer}$ is the maximum transient observed for the $[Ru(bpy)_3]^{2+}$ actinometer under identical excitation conditions and $\Delta\varepsilon_{actinometer} \sim 22{,}000\ M^{-1}cm^{-1}$ as previously reported[13,14]. Both sample and actinometer had absorbance ~ 0.35, and the fraction quenched was calculated by extrapolation from the Stern-Volmer constant.

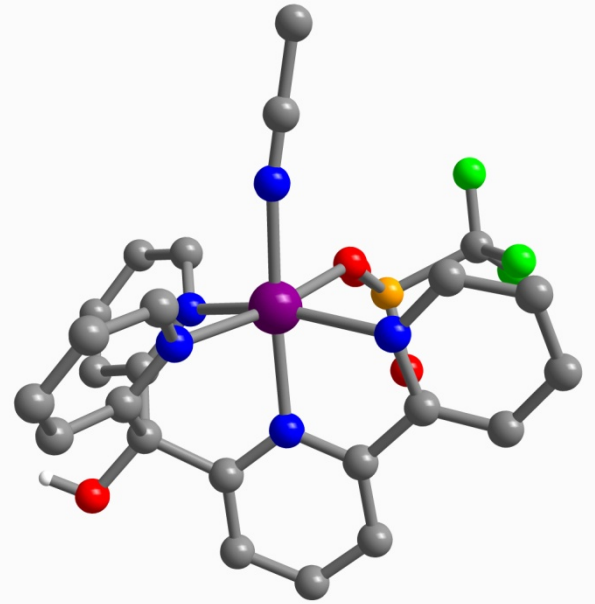

Fig. S1 Molecular structure of the monocationic Co complex in the crystal structure of **4**. Purple, blue, grey, red, orange, and green spheres represent Co, N, C, O, S, and F atoms, respectively; hydrogen atoms (except for OH) have been omitted for clarity.

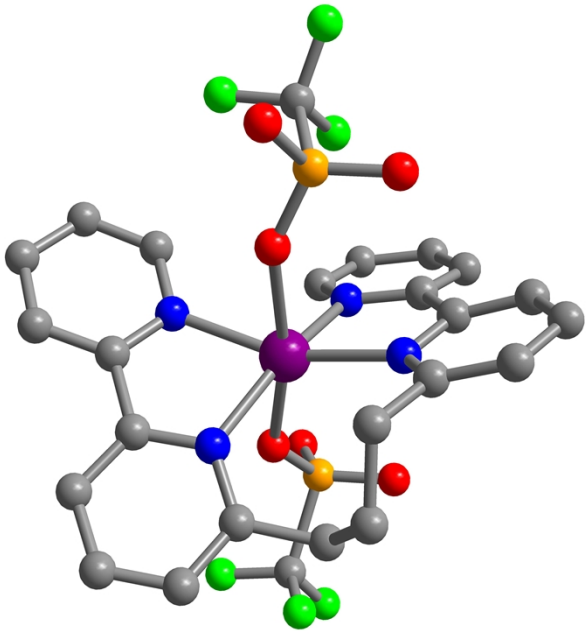

Fig. S2 Molecular structure of [Co(pr-bpy2)(SO_3CF_3)$_2$] **(6)**. Purple, blue, grey, red, orange, and green spheres represent Co, N, C, O, S, and F atoms, respectively; hydrogen atoms have been omitted for clarity.

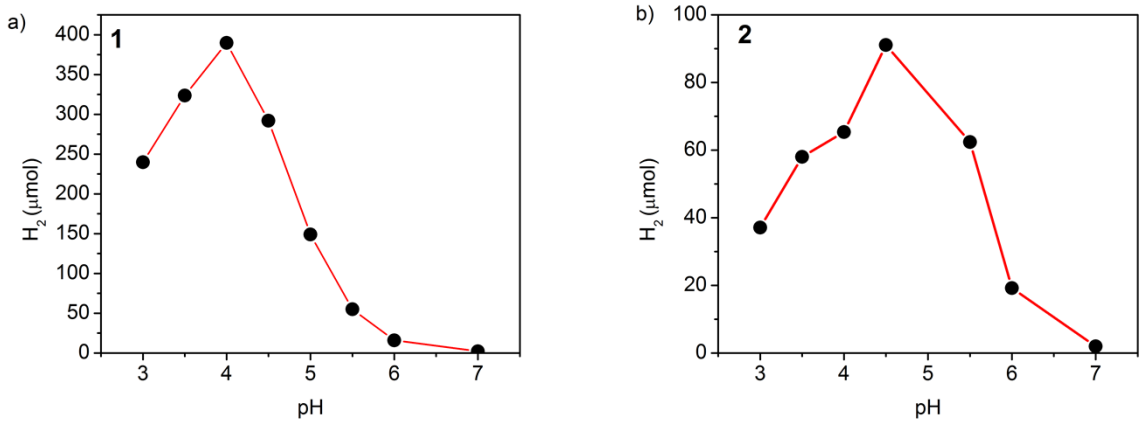

Fig. S3 pH dependence on total H_2 production collected after hydrogen production ceases for a) **1** and b) **2**. Conditions: 2.0 x 10^{-5} M of catalyst, 3.3 x 10^{-4} M $[Ru(bpy)_3]^{2+}$ and 0.3 M H_2A/HA^-.

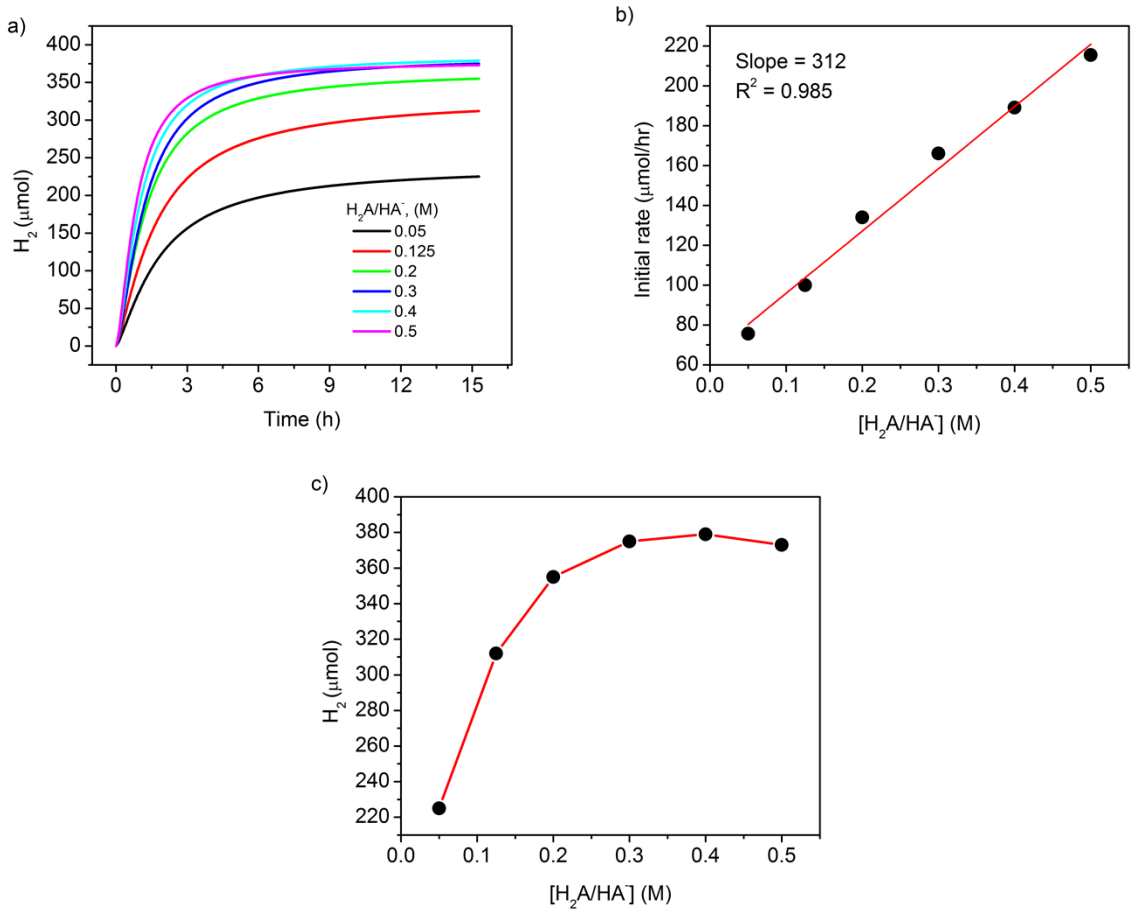

Fig. S4 a) H_2 production kinetic curves, b) initial rate of hydrogen production, and c) total H_2 produced collected after the reactions cease as a function of H_2A/HA^- concentration. Conditions: 2.0 x 10^{-5} M **1**, 3.3 x 10^{-4} M $[Ru(bpy)_3]^{2+}$ at pH 4.

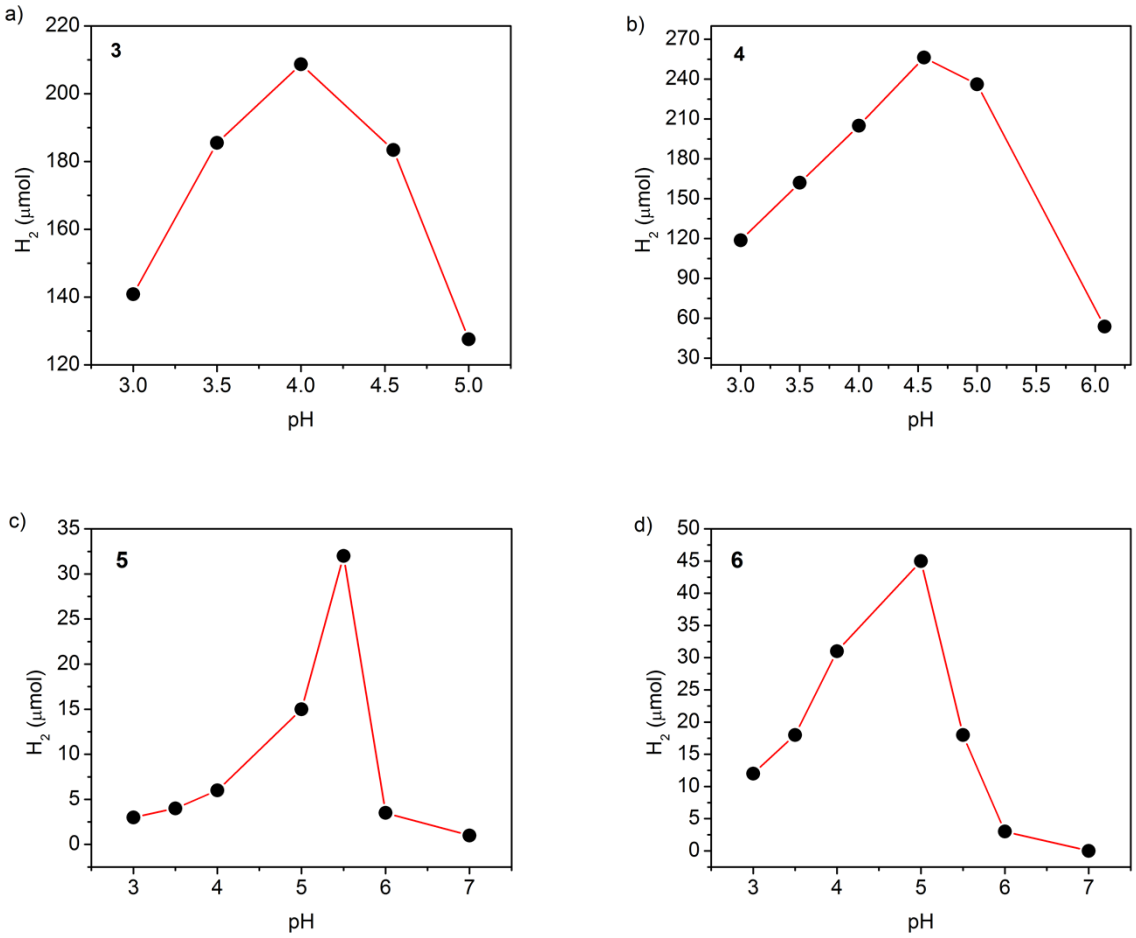

Fig. S5 pH dependence on H_2 production collected after H_2 production ceases for a) **3**, b) **4**, c) **5**, and d) **6**. Conditions: 2.0 x 10^{-5} M of catalyst, 3.3 x 10^{-4} M $[Ru(bpy)_3]^{2+}$ and 0.3 M H_2A/HA^-.

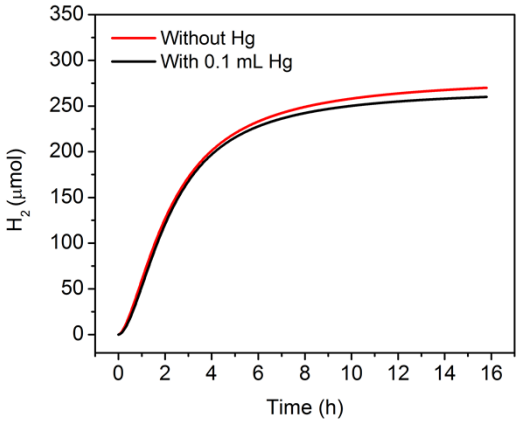

Fig. S6 Mercury poisoning test performed on a sample containing 2.5 x 10^{-5} M **1**, 3.3 x 10^{-4} M $[Ru(bpy)_3]^{2+}$ and 0.1 M H_2A/HA^- at pH 4.

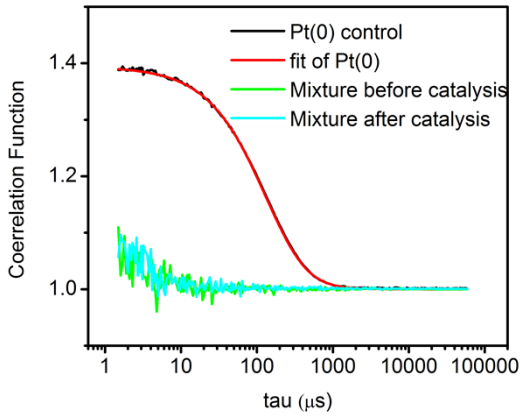

Fig. S7 Dynamic light scattering (DLS) before (green) and after (cyan) a 30 minutes of irradiation of a solution containing 1.5 x 10^{-5} M $[Ru(bpy)_3]^{2+}$ and 4 x 10^{-5} M **1** in 0.5 M H_2A/HA^-, pH 4. The Pt(0) nanoparticles (black) were grown chemically by chemical reduction ($NaBH_4$) of a platinum precursor in water and used as standards at ~ 10^{-5}-10^{-4} M. This figure shows clear light scattering for the Pt(0) particles along with its autocorrelation function fit (red). No light scattering was detected from our photocatalytic mixture before and after irradiation indicating the lack of formation of nanoparticles beyond 1 nm in diameter in the catalytic solution.

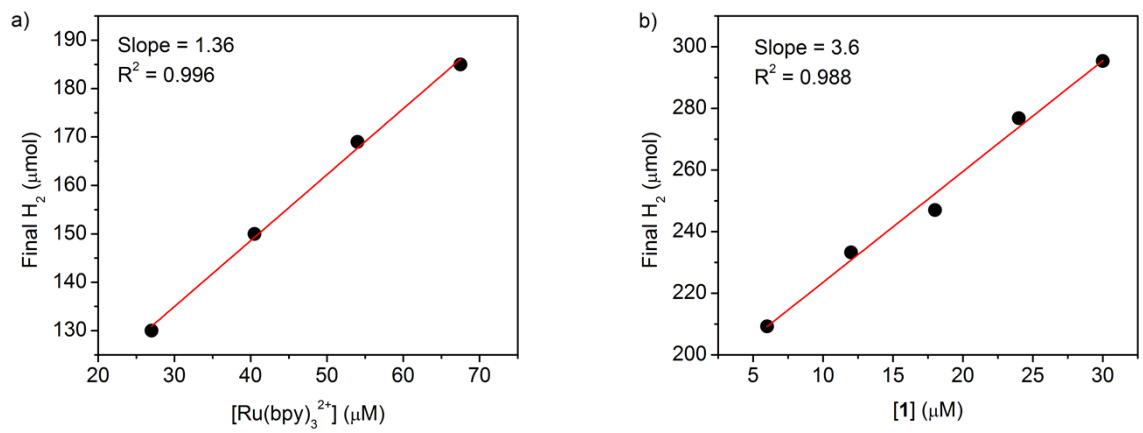

Fig. S8 Linear dependence of final hydrogen produced as a function of a) $[Ru(bpy)_3]^{2+}$ concentration at 2.0 x 10^{-5} M **1**, and as a function of b) **1** concentration at 3.3 x 10^{-4} M $[Ru(bpy)_3]^{2+}$. These experiments were performed in 0.1 M H_2A/HA^- at pH 4 in water. Under these conditions, the rate of hydrogen production is independent on the concentration of PS and catalyst, the rate is mainly limited by light absorption and subsequent electron transfer. However the stability and the overall hydrogen produced after the reaction ceases increases with the increase of **1** and $[Ru(bpy)_3]^{2+}$.

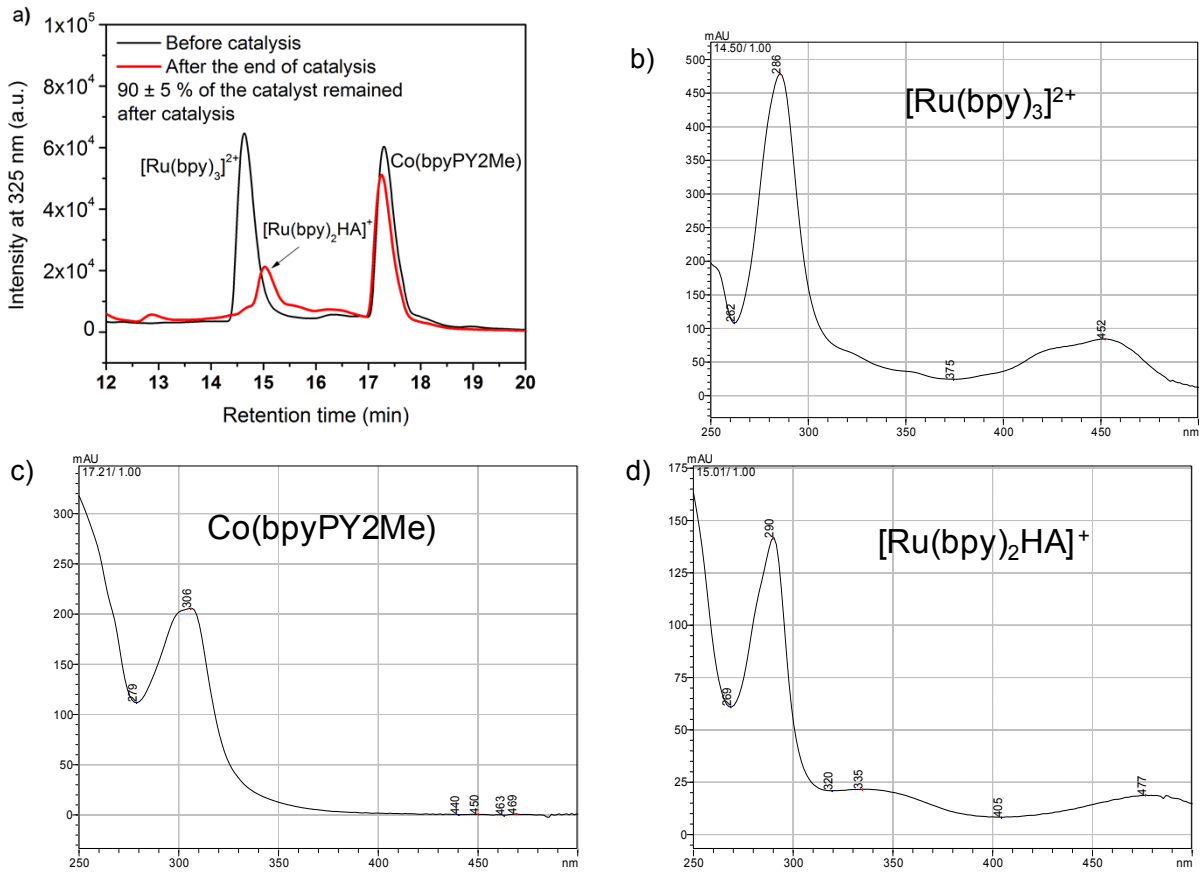

Fig. S9 This experiment was performed with a solution of 4 x 10^{-5} M **1**, 1.5 x 10^{-5} M $[Ru(bpy)_3]^{2+}$ and 0.5 M H_2A/HA^- at pH 4. Measurements were taken before and after 1.5 hours of irradiation using LED light (452 ± 10 nm, 540 mW). HPLC was perfomed on a Shimadzu instrument equiped with a PDA detector, using C18 analytical column for seperation. Mobile phase: H_2O and MeOH containing 0.1 % trifluoroacetic acid (TFA). Gradient: 10-90 % MeOH over a period of 40 min, the flow rate was 0.1 mL/min. Figure a) represents the LC trace of the injected sample monitored at λ_{abs} = 325 nm, whereas the rest represent the absorption spectra of corresponding to the following peaks labeled peaks of the LC trace: b) $[Ru(bpy)_3]^{2+}$ photosensitizer, c) Co(bpyPY2Me) catalyst or **1**, and d) the $[Ru(bpy)_2HA]^+$ photoproduct isolated after catalysis.

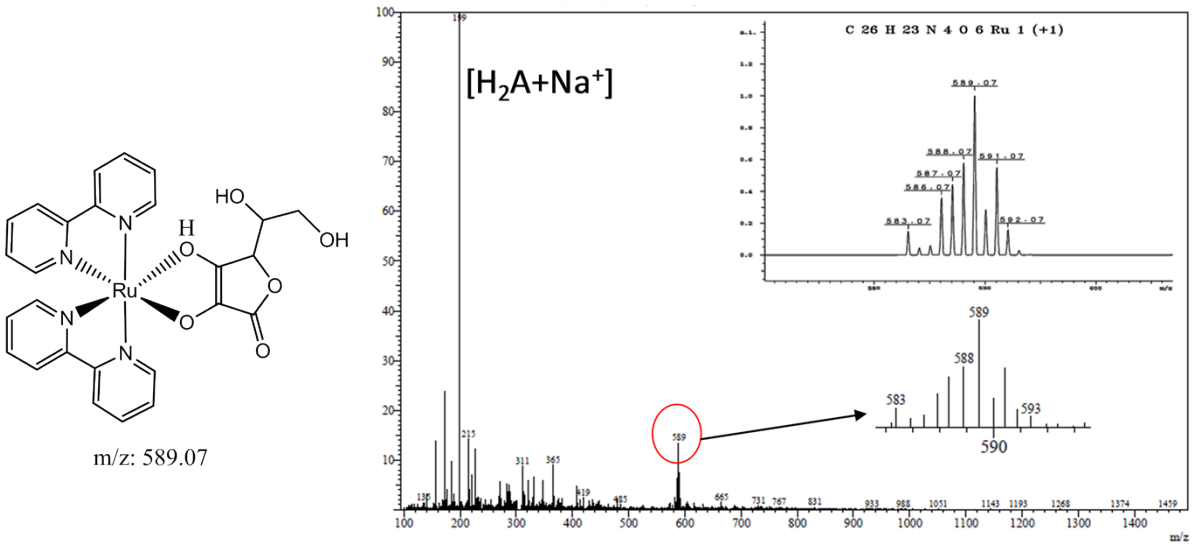

Fig. S10 ESI-positive (LC-MS) of a photocatalytic sample after 18 h of photo catalysis indicating the presence of $[Ru(bpy)_2HA]^+$. Initial conditions: 2 x 10^{-5} M **1**, 1 x 10^{-4} M $[Ru(bpy)_3]^{2+}$ and 0.3 M H_2A/HA^-, pH 4. The inset on top is a simulation of the molecular ion peak which matches the experimental data (bottom) for isotopic distribution.

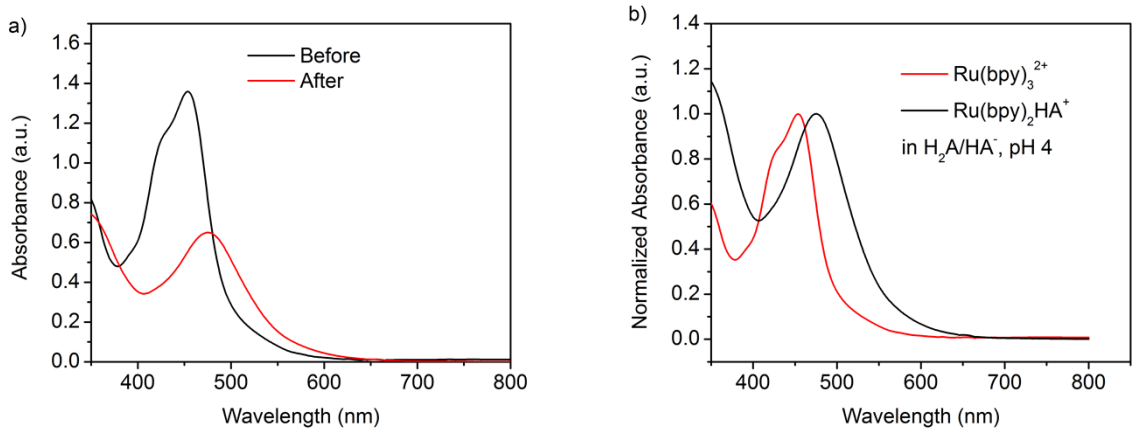

Fig. S11 a) UV-Vis of the photocatalytic composition before (black) and after (red) ~ 18 h of photocatalysis. b) Normalized absorbance of $[Ru(bpy)_3]^{2+}$ (black) and $[Ru(bpy)_2HA]^{+}$ (red). Initial conditions: 2 x 10^{-5} M **1**, 1 x 10^{-4} M $[Ru(bpy)_3]^{2+}$ and 0.3 M H_2A/HA^- at pH 4.

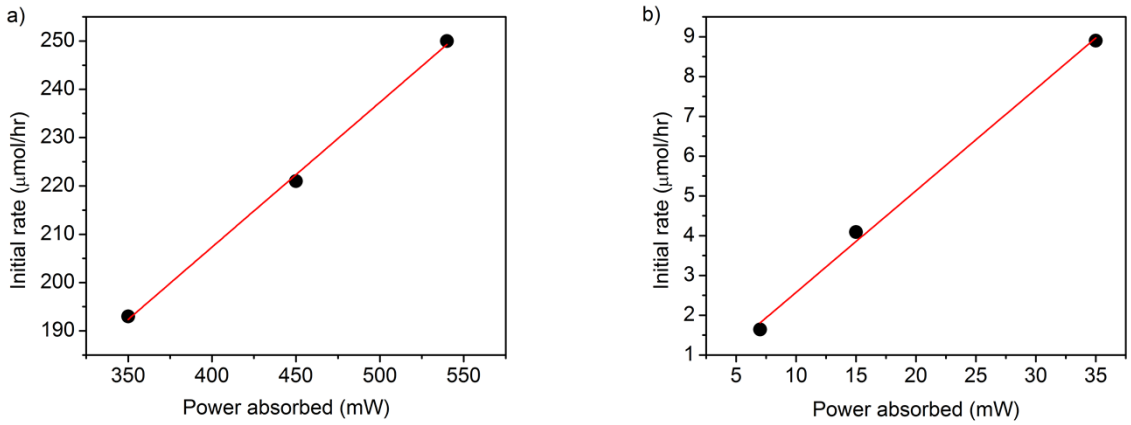

Fig. S12 Hydrogen produced as a function of optical power absorbed by the samples using a) LED as light source (452 ± 10 nm), 4 x 10^{-5} M **1**, 3.3 x 10^{-4} M $[Ru(bpy)_3]^{2+}$ and 0.5 M H_2A/HA^- at pH 4, and b) He/Cd as light source (442 nm), 1.5 x 10^{-5} M $[Ru(bpy)_3]^{2+}$, 4 x 10^{-5} M **1**, 0.5 M H_2A/HA^- at pH 4.

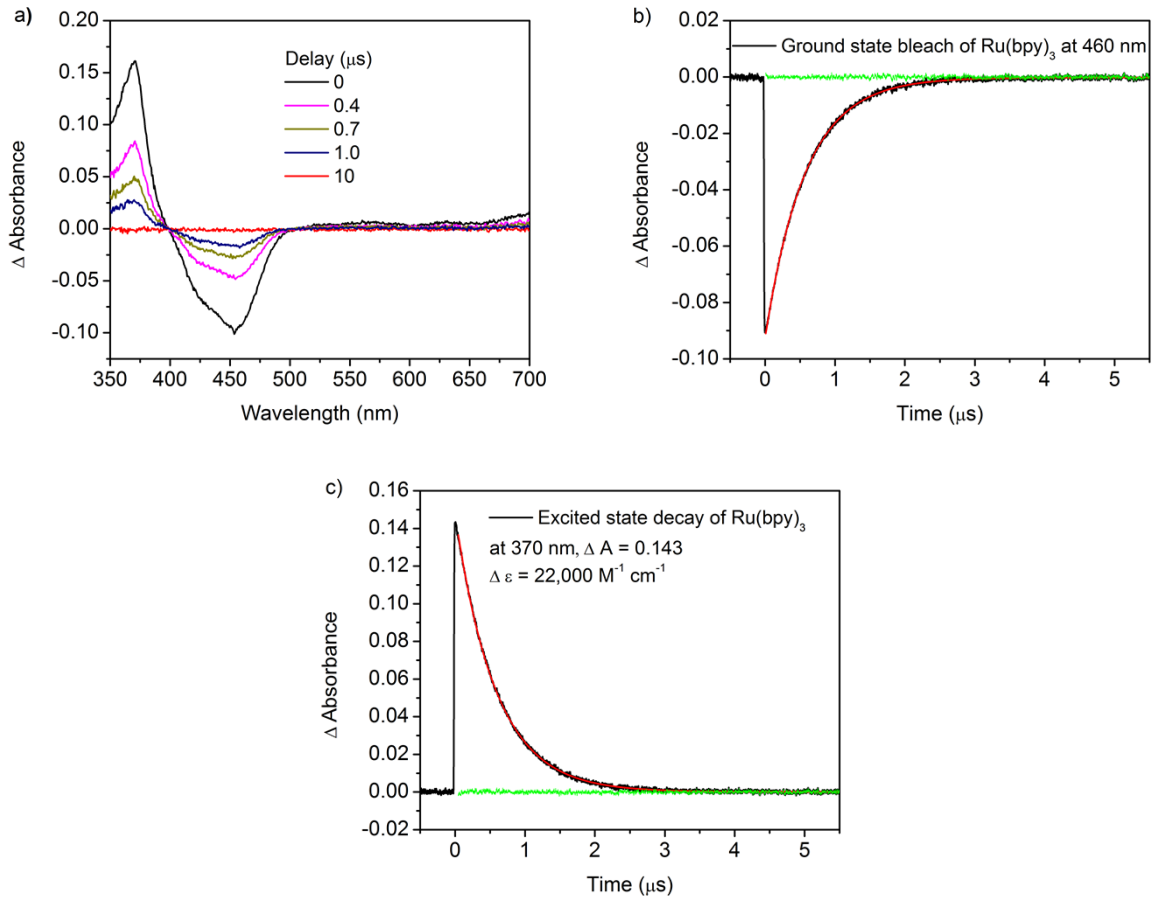

Fig. S13 a) Transient absorption of $[Ru(bpy)_3]^{2+}$ in water ($A_{452\ nm}$ ~ 0.35, H_2O), excited with a 452 nm laser Nd:YAG (~ 5 mJ/pulse). b) Ground-state bleach recovery measured at 460 nm with lifetime of ~ 0.6 μs**.** c) Excited state absorption decay at 370 nm where the $\Delta\varepsilon_{max}$ ~ 22,000 $M^{-1}cm^{-1}$.[13,14] The green data points represent the residual of the exponential decay fit.

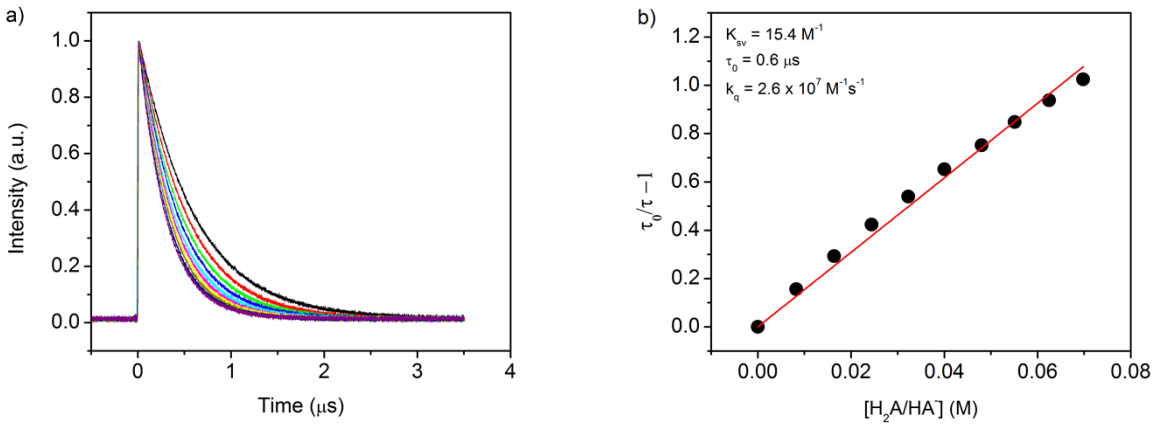

Fig. S14 a) Dynamic photoluminescence quenching of the emission intensity vs time measured at emission wavelength of 610 ± 2 nm in H_2O as a function of added H_2A/HA^- from a stock solution at pH 4. b) Stern-Volmer plot of the lifetime data.

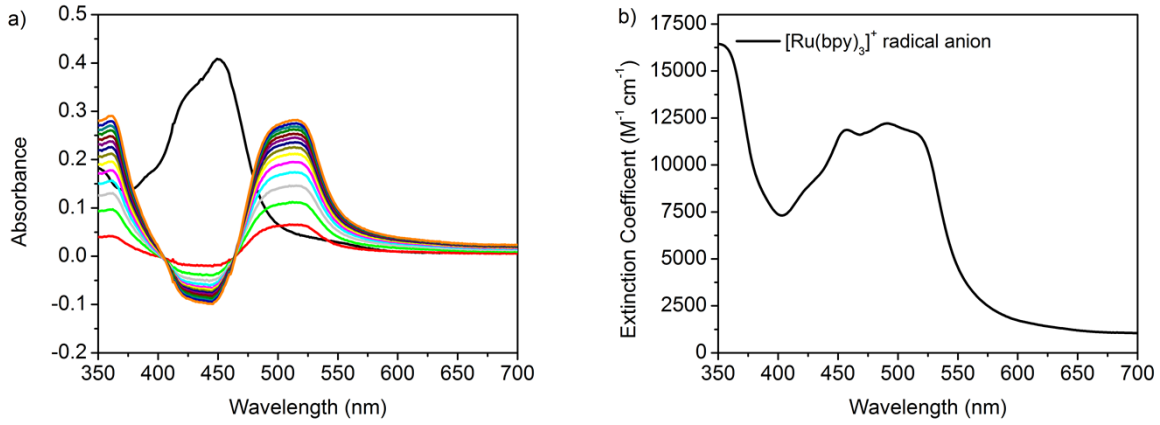

Fig. S15 a) Spectroelectrochemical spectra of 2.8 x 10^{-4} M $[Ru(bpy)_3]^{2+}$ in ACN (0.1 M $TBAPF_6$ supporting electrolyte, -1750 mV applied potential vs $Ag/AgNO_3$) as a function of time of electrolysis (0.5 minute interval going from red to dark yellow spectrum). The black spectrum represents the absorption of $[Ru(bpy)_3]^{2+}$ before the experiment. Note that the absorption of initial $[Ru(bpy)_3]^{2+}$ was blanked before the start of electrolysis. b) Extinction coefficient of $[Ru(bpy)_3]^{2+}$ deduced from the SEC data after the end of electrolysis following the Beer-Lambert law.

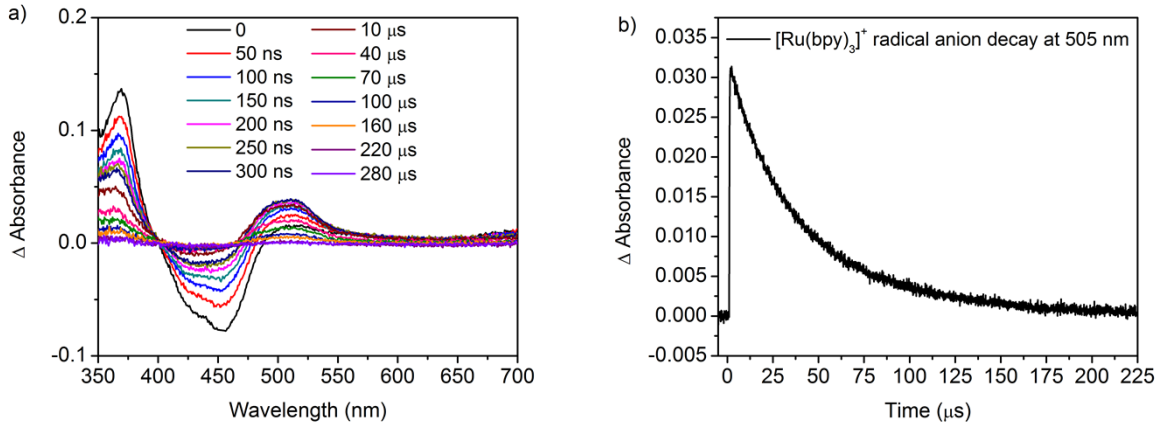

Fig. S16 a) Transient absorption of $[Ru(bpy)_3]^{2+}$ in 0.3 M H_2A/HA^- ($A_{452\ nm}$ ~ 0.35, pH 4), excited with a 452 nm laser Nd:YAG (~ 5 mJ/pulse). b) Kinetic decay of the $[Ru(bpy)_3]^{+}$ radical anion at 505 nm indicating a complete recombination with $HA^{\cdot}$.

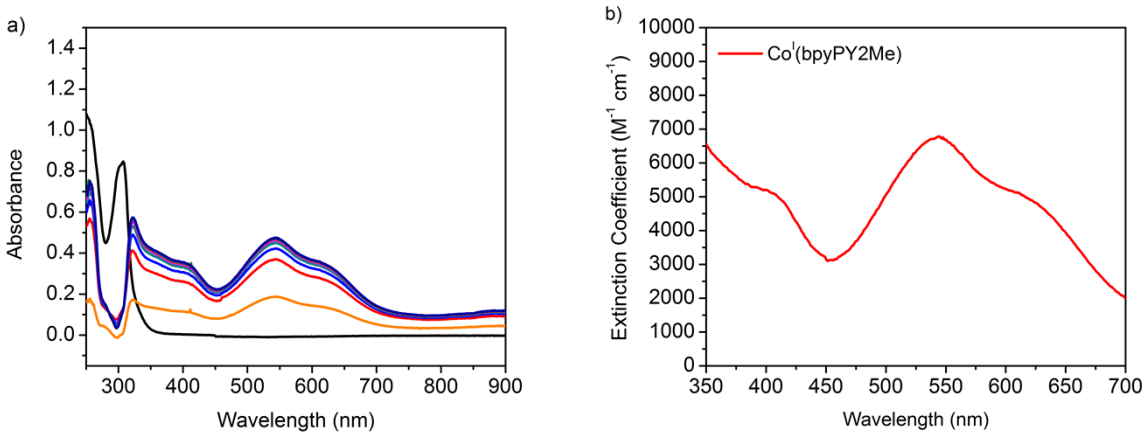

Fig. S17 a) Spectroelectrochemical spectra of 6.8 x 10^{-4} M **1** in ACN (0.1 M $TBAPF_6$ supporting electrolyte, -1250 mV vs $Ag/AgNO_3$) as a function of time of electrolysis (1 minute time interval from the orange to deep blue spectrum). The black spectrum represents the absorption of Co^{II}(bpyPY2Me) before the experiment. Note that the absorption of Co^{III}(bpyPY2Me) was blanked before the start of electrolysis. b) Extinction coefficient of Co^{I}(bpyPY2Me) deduced from the SEC data after the end of electrolysis following the Beer-Lambert law.

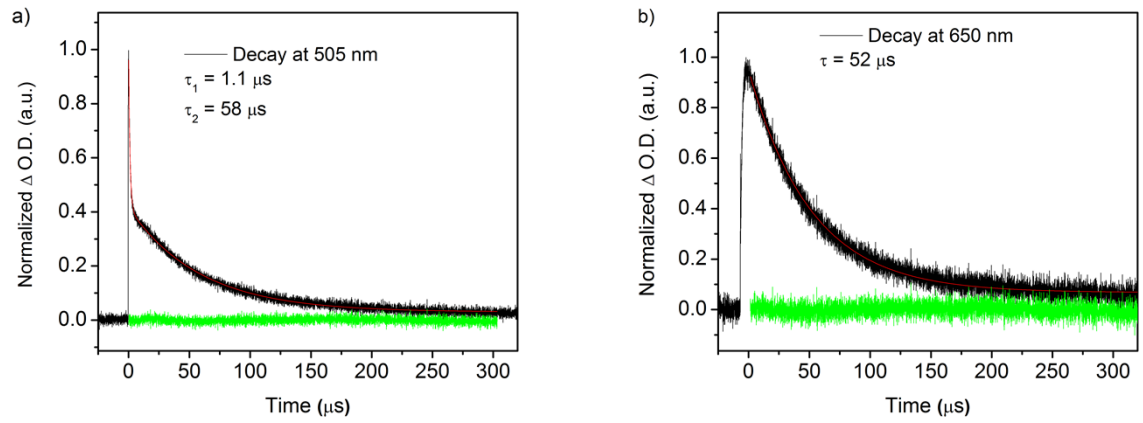

Fig. S18 Kinetic transient absorption decay monitored at a) 505 nm and b) 650 nm. Conditions: 4.4 x 10^{-4} M **1**, 2.5 x 10^{-5} $[Ru(bpy)_3]^{2+}$ in 0.3 M H_2A/HA^- at pH 4. The green data points represent the residual of the exponential decay fit.

Electrochemical Characterization of 7-9.

The static cyclic (Figure S19) and rotating disk electrode (RDE) voltammograms (Figure S20 right) of **7-9** measured at pH 7 qualitatively support the activity trends obtained from photocatalytic experiments with **7** showing the highest catalytic current. Although **9** exhibits the least negative onset potential for water reduction, the current quickly levels off at more negative potentials. The direct catalytic onset and lack of catalytic prefeatures observed for **7-9** contrasts the electrochemical behavior of $[(PY5Me_2)Co(H_2O)]^{2+}$ and suggests that these catalysts can directly operate from the Co^{1+} state even at neutral pH. The cobalt-catalyzed water reduction processes are diffusion-limited at -1.2 V as shown by the linear dependence of the current density on rotation rate in RDE experiments (see Figure S21 for Levich plot). Controlled potential electrolysis conducted at -1.2 V (Figure 12 inset) further confirms higher activity for **7** than for **8** with moderate TONs of 60 and 44 (after 3h), respectively, with 100 % Faradaic efficiency. The significantly lower activity and reduced Faradaic efficiency (84 %) observed for **9**, suggest the presence of competing pathways in its reductive chemistry.

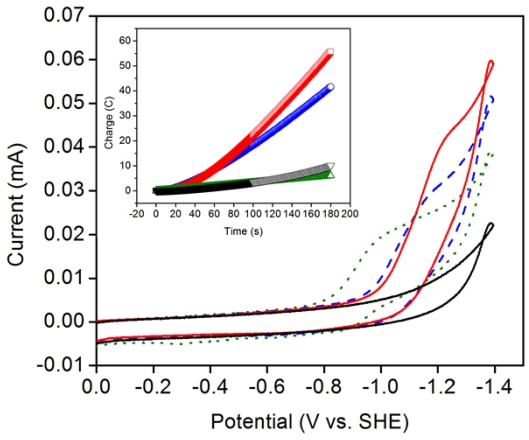

Fig. S19 Cyclic voltammograms in the absence (black) and presence of 0.5 mM of complex **7** (red), **8** (blue dashes), and **9** (green dots) in a 0.3 M ascorbate at pH 7 under an inert atmosphere, using a glassy carbon disk electrode at a scan rate of 100 $mV \cdot s^{-1}$ (CV). Inset: charge accumulated over time in a controlled potential electrolysis at −1.2 V vs. SHE in the absence (black) and presence of 5 x 10^{-4} M of complex **7** (red), **8** (blue), and **9** (green) in a 0.3 M ascorbate at pH 7 under an inert atmosphere, using a glassy carbon disk electrode.

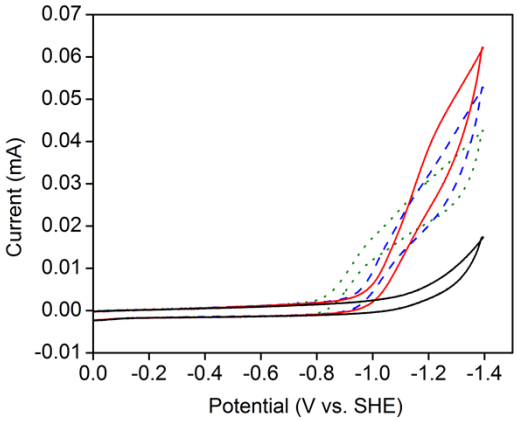

Fig. S20 RDE voltammograms in the absence (black) and presence of 0.5 mM of complex **7** (red), **8** (blue dashes), and **9** (green dots) in a 0.3 M ascorbic acid at pH 7 under an inert atmosphere, using a glassy carbon disk electrode at a scan rate of 25 $mV \cdot s^{-1}$.

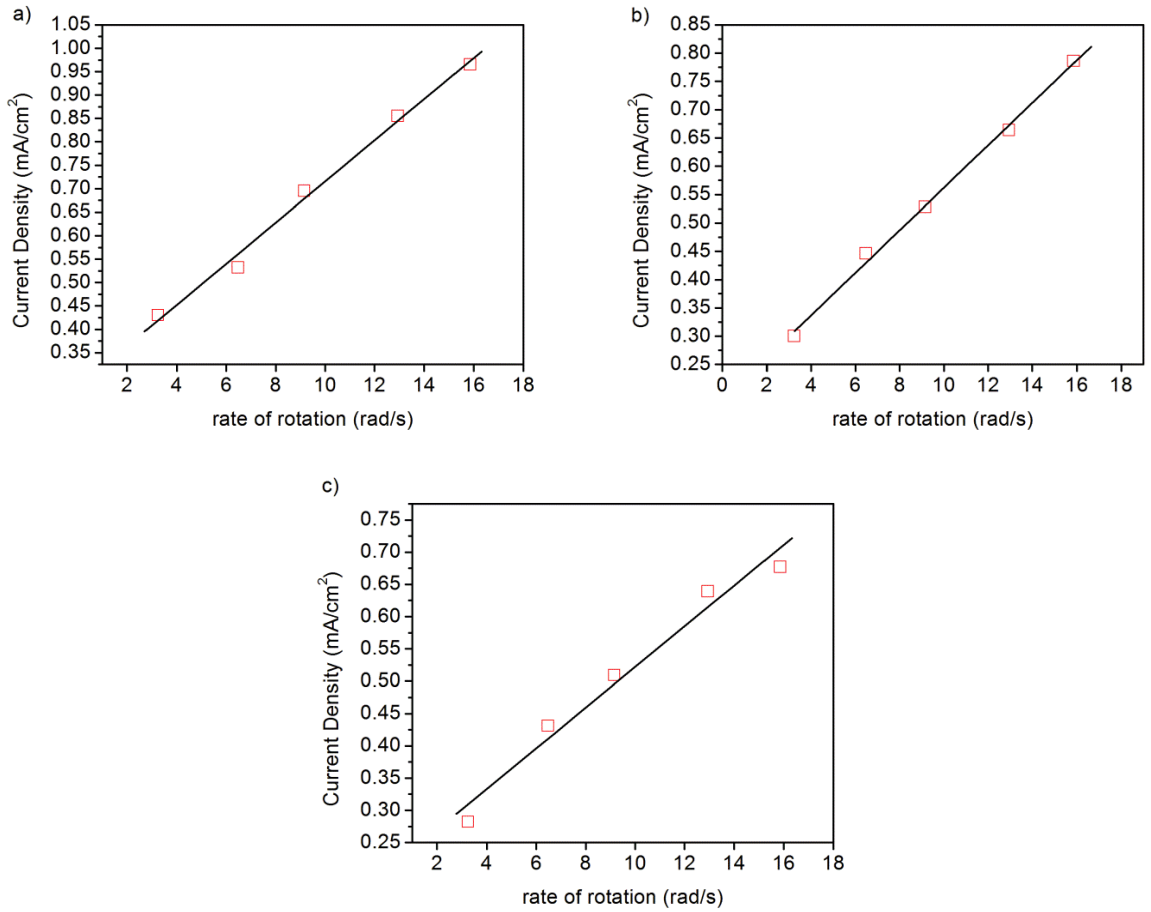

Fig. S21 Linear Levich plots at −1.2 V of 0.5 mM of complex a) **7**, b) **8**, and c) **9** in a 0.3 M ascorbic acid at pH 7 under an inert atmosphere, using a glassy carbon disk electrode at a scan rate of 25 mV·s^{-1}.

Photochemical Characterization of 7.

MS analysis of the gas in the headspace established that H_2 is the main product produced in the first 18 h of photocatalysis. However, after 18 h of catalysis, the rate of H_2 evolution decreases while the production of CO_2 increases as a result of ascorbic acid decomposition (Figure S24).[15,16] Time resolved pump-probe spectroscopy experiments at pH 7 were utilized to evaluate some of the relevant rate constants for the photocatalytic system. Overall, the system characteristics utilizing **7** at pH 7 mimic those as described above for **1** at pH 4. Based on our findings we propose the photocatalytic cycle shown in Scheme 4. Excitation of $[Ru(bpy)_3]^{2+}$ results in formation of $^3[Ru(bpy)_3]^{2+*}$ which displays a life time of 0.6 µs in the absence of an artificial reductand. In the presence of H_2A/HA^-, $^3[Ru(bpy)_3]^{2+*}$ is reductively quenched with $k_q = 2.6 \cdot 10^7\ M^{-1}s^{-1}$ and a cage escape yield of 55 % for the photosensitizer/catalyst electron transfer pair. Electron transfer from $[Ru(bpy)_3]^+$ to **1** at pH 4 was determined to be somewhat faster ($k_1 = 2 \times 10^9\ M^{-1}s^{-1}$) than to **7** at pH 7 ($k_7 = 7.8 \times 10^8\ M^{-1}s^{-1}$).

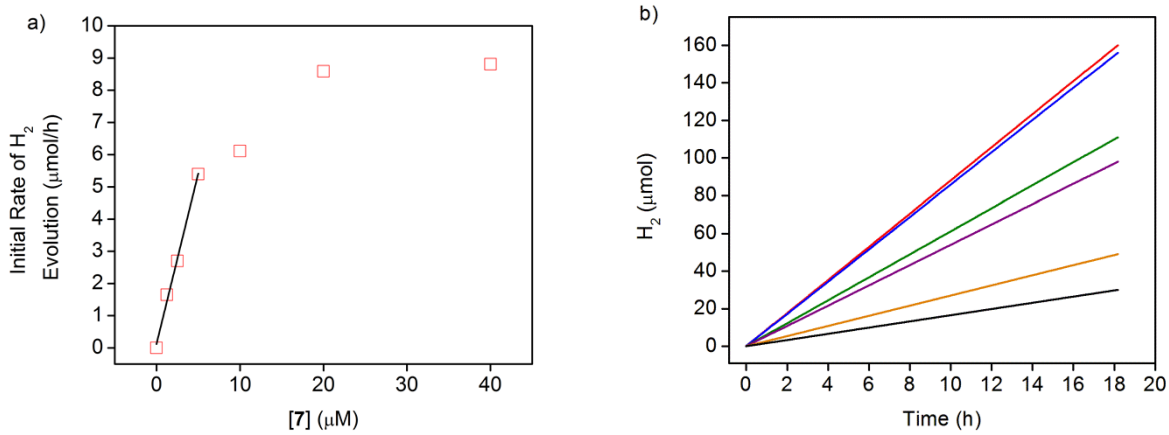

Fig. S22 a) Initial hydrogen production rates as a function of concentration of **7** and b) kinetic traces at 0.3 M ascorbate at pH 7 containing 0.33 mM $[Ru(bpy)_3]Cl_2$ and 40 µM (red), 20 µM (blue), 10 µM (green), 5 µM (purple), 2.5 µM (orange), and 1.25 µM (black) of **7** under an inert atmosphere.

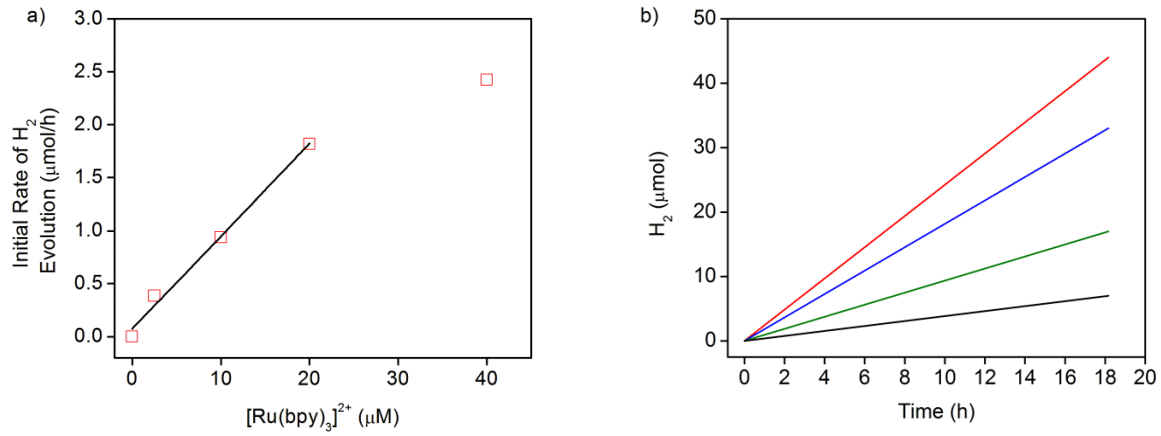

Fig. S23 a) Initial hydrogen production rates as a function of concentration of $[Ru(bpy)_3]Cl_2$ and b) kinetic traces at 0.3 M ascorbate at pH 7 containing 0.02 mM of **7** and 40 μM (red), 20 μM (blue), 10 μM (green), 5 μM (purple), 2.5 μM (orange), and 1.25 μM (black) of $[Ru(bpy)_3]Cl_2$ under an inert atmosphere.

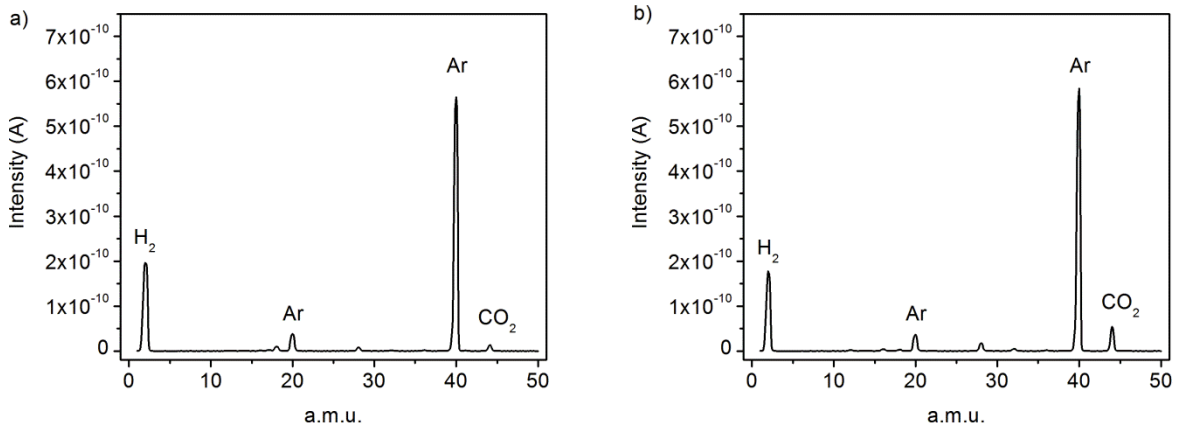

Fig. S24 Mass spectrometry sampling of the headspace of two independent photoreactions terminated after a) 18 h and b) 60 h of catalysis. Conditions: 0.02 mM of complex **7** in a 0.3 M ascorbate at pH 7 containing 0.33 mM $[Ru(bpy)_3]Cl_2$ under an inert atmosphere. Note that the headspace was always equilibrated close to atmospheric pressure by an oil bubbler to accurately measure the percent of each gas relative to Ar which was used as our internal standard.

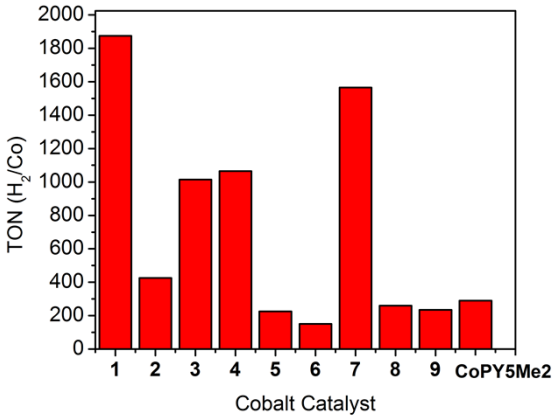

Fig. S25 Photocatalytic turnover numbers (H_2/Co) under 452 ± 10 nm (540 mW) of a solution containing 2 x 10^{-5} M **1** (pH 4.0), **2** (pH 4.5), **3** (pH 4.5), **4** (pH 4.0), **5** (pH 5.5), **6** (pH 5.0), **7** (pH 5.0), **8** (pH5.5) **9** (pH 5.0), and the prototypical CoPY5Me2 (pH 6.0), 3.3 x 10^{-4} M $[Ru(bpy)_3]^{2+}$ in 0.3 M H_2A/HA^-. All these values are extracted after hydrogen evolution ceases as verified by mass spectrometry and gas chromatography.

Scheme S1. Proposed photocatalytic cycle for hydrogen evolution. Please note that H_2 evolution is a 2 e^- process and the drawn cycle is a one photon/one electron cycle.

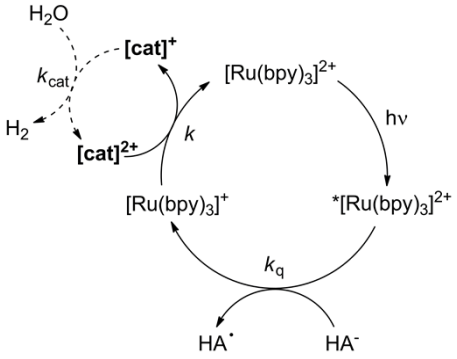

Table S1. Crystallographic data for Co complexes **1**, **2**, **4**, and **6**.

Compound	1	2	4	6
Formula	$C_{26}H_{21}CoF_6N_5O_6S_2$	$C_{33}H_{26.50}CoF_{12}N_{7.50}O_6S_2$	$C_{27}H_{22}CoF_6N_6O_7S_2$	$C_{16.67}H_{13.33}Co_{0.67}F_4N_{2.67}O_4S_{1.33}$
Crystal system	Triclinic	Triclinic	Triclinic	Monoclinic
Space group	P-1	P-1	P-1	P2(1)/n
a, Å	8.0983(6)	16.288(3)	8.3555(5)	12.0052(15)
b, Å	12.4502(9)	16.463(3)	13.6865(8)	17.117(2)
c, Å	15.5631(12)	17.020(3)	15.1917(8)	13.5392(17)
α, °	105.7600(10)	62.683(2)	116.451(2)	90
β, °	103.1140(10)	83.145(2)	94.117(2)	99.567(2)
γ, °	101.1240(10)	83.634(2)	90.678(3)	90
V, Å^3	1415.50(18)	4017.8(10)	1549.54(15)	2743.5(6)
Z	2	4	2	6
ρ, Mg m^{-3}	1.728	1.612	1.671	1.718
R1[a], *w*R2[b] ($I > 2\sigma(I)$)	0.0253, 0.0637	0.0780, 0.1962	0.0275, 0.1129	0.0296, 0.0701
R1[a], *w*R2[b] (all data)	0.076, 0.0658	0.1652, 0.2459	0.0302, 0.1182	0.0317, 0.0717

[a]$R1 = 3||F_o| - |F_c||/3|F_o|$. [b]$wR2 = [3[w(F_o^2 - F_c^2)^2]/3[w(F_o^2)^2]]^{½}$, $w = 1/\sigma^2(F_o^2) + (aP)^2 + bP$, where $P = [\max(0 \text{ or } F_o^2) + 2(F_c^2)]/3$.

Table S2. Crystallographic data for Co complexes **7**, **8**, and **9**.

Compound	7	8	9
Formula	$C_{27}H_{23}CoF_6N_5O_6S_2$	$C_{26}H_{28}CoF_6N_4O_9S_2$	$C_{30.50}H_{27}CoF_6N_6O_6S_2$
Crystal system	Monoclinic	Triclinic	Monoclinic
Space group	P2(1)/c	P-1	I2/a
a, Å	12.8142(5)	9.6468(5)	24.9411(13)
b, Å	16.9334(6)	11.9557(6)	11.4329(4)
c, Å	13.8652(6)	14.9502(8)	26.1884(9)
a, °	90	105.694(3)	90
β, °	98.362(2)	105.787(3)	116.585(2)
g, °	90	100.066(3)	90
V, Å^3	2976.6(2)	1538.89(14)	6678.1(5)
Z	4	2	8
ρ, Mg m^{-3}	1.675	1.678	1.613
R1[a], *w*R2[b] ($I > 2\sigma(I)$)	0.0277, 0.0660	0.0303, 0.0716	0.0610, 0.1393
R1[a], *w*R2[b] (all data)	0.0297, 0.0672	0.0322, 0.0727	0.1204, 0.1675

[a]$R1 = 3||F_o| - |F_c||/3|F_o|$. [b]$wR2 = [3[w(F_o^2 - F_c^2)^2]/3[w(F_o^2)^2]]^{½}$, $w = 1/\sigma^2(F_o^2) + (aP)^2 + bP$, where $P = [\max(0 \text{ or } F_o^2) + 2(F_c^2)]/3$.

Table S3. Crystallographic bond distances and angles for complexes **1**, **2**, **4**, and **6.**

Complexes	Avg M-N_{bpy} (Å)	Avg M-N_{py} (Å)	M-L (Å), L_{ax}
1	2.071[2]	2.093[2]	2.069(2), CH_3CN; 2.269(2), $(SO_3CF_3)^-$
2	2.092[5]	2.121[5]	2.108[6], CH_3CN
4	2.106[2]	2.116[2]	2.088(2), CH_3CN; 2.189(1), $(SO_3CF_3)^-$
6	2.129[2]	–	2.228[2], $(SO_3CF_3)^-$

Table S4. Crystallographic bond distances and angles for complexes **7**-**9**.

Complexes	Avg M-N_{py} (Å)	M-L_{eq} (Å), L_{eq}	M-L_{ax} (Å), L_{ax}	$N_{py,eq}$-M-H (°)	$N_{py,ax}$-M-H (°)
7	2.116[2]	2.190(1), $(SO_3CF_3)^-$	2.123(2), CH_3CN	n/a	n/a
8	2.113[2]	2.314(1), $(SO_3CF_3)^-$	2.078(2), H_2O	n/a	n/a
9	1.980[4]	2.185, refined H	1.919(4), CH_3CN	83.9(2), 85.7(2), 170.6(2)	82.4(2)

References

1 J. P. Bigi, T. E. Hanna, W. H. Harman, A. Chang, C. J. Chang, *Chem. Commun.* 2010, **46**, 958.
2 K. M. Lam, K. Y. Wong, S. M. Yang, C. M. Che, *J. Chem. Soc., Dalton Tans.* 1995, 1103.
3 M. Guttentag, A. Rodenberg, C. Bachmann, A. Senn, P. Hamm, R. Alberto, *Dalton Trans.* 2012, **42**, 334.
4 M. Nippe, R. S. Khnayzer, J. A. Panetier, D. Z. Zee, B. S. Olaiya, M. Head-Gordon, C. J. Chang, F. N. Castellano, J. R. Long, *Chem. Sci.* 2013, **4***,* 3934.
5 W. Zambach, L. Quaranta, C. Massol-Frieh, S. Trah, D. Stierli, M. Pouliot, K. Nebel, International Patent WO2013026866 (A2) - Novel Microbiocides.
6 A. J. Canty, N. J. Minchin, B. W. Skelton, A. H. White, *J. Chem. Soc., Dalton Trans.* 1986, 2205.
7 E. A. Ünal, D. Wiedemann, J. Seiffert, J. P. Boyd, A. Grohmann, *Tetrahedron Lett.* 2012, **53**, 54.
8 Y. Sun, J. P. Bigi, N. A. Piro, M. L. Tang, J. R. Long, C. J. Chang, *J. Am. Chem. Soc.* 2011, **133**, 9212.
9 *APEX2, v. 2009; Bruker Analytical X-Ray Systems, Inc: Madison, WI, 2009*.
10 G. M. Sheldrick, SADABS, Version 2.03; Bruker Analytical X-ray Systems, Inc: Madison, WI, 2000.
11 O. V. Dolomanov, L. J. Bourhis, R. J. Gildea, J. A. K. Howard, H. Puschmann, *J. Appl. Cryst.* 2009, **42**, 339.
12 R. S. Khnayzer, C. E. McCusker, B. S. Olaiya, F. N. Castellano, *J. Am. Chem. Soc.* 2013, **135**, 14068.
13 M. Ruthkosky, F. N. Castellano, G. J. Meyer, *Inorg. Chem.* **1996**, *35*, 6406.
14 T. E. Mallouk, J. S. Krueger, J. E. Mayer, C. M. G. Dymond, *Inorg. Chem.* 1989, **28**, 3507.
15 G. Patkai, I. Kormendy, A. Kormendy-Domjan, *Acta Aliment. Hung.* 2002, **31**, 125.
16 J. R. Lima, N. J. Elizondo, P. Bohuon, *Int. J. Food Sci. Tech.* 2010, **45**, 1724.